Biogeosciences Discuss., https://doi.org/10.5194/bg-2018-304
Manuscript under review for journal Biogeosciences
Discussion started: 24 July 2018

Limited impact of El Niño – Southern Oscillation on the methane cycle

Hinrich Schaefer[1], Dan Smale[1], Sylvia E. Nichol[1], Tony M. Bromley[1], Ross J. Martin[1], Rowena Moss[1], Sylvia Englund Michel[2], James W. C. White[2]

[1]Climate and Atmosphere Centre, National Institute of Water and Atmospheric Research, Wellington, 6021, New Zealand
[2] Institute of Arctic and Alpine Research, Boulder, CO, USA.

Correspondence to: Hinrich Schaefer (Hinrich.Schaefer@niwa.co.nz)

2. Abstract. The El Niño – Southern Oscillation (ENSO) has been suggested as a strong forcing in the methane cycle and as a driver of recent trends in global atmospheric methane levels. Such a sensitivity of the global CH_4 budget to climate events would have important repercussions for climate change mitigation strategies and the accuracy of projections for future greenhouse forcing. Here, we test the impact of ENSO on the CH_4 cycle in a correlation analysis. We use local and global records of methane mixing ratio [CH_4], as well as stable carbon isotopic records of atmospheric CH_4 ($\delta^{13}CH_4$), which are particularly sensitive to the combined ENSO effects on CH_4 production from wetlands and biomass burning. We use a variety of nominal, smoothed and detrended time series including growth rate records. We find that at most 36% of the variability in [CH_4] and $\delta^{13}CH_4$ is attributable to ENSO, but only for detrended records in the Southern tropics. Trend-bearing records from the Southern tropics, as well as all studied hemispheric and global records show a minor impact of ENSO, i.e. <28% of variability explained. Additional analyses using hydrogen cyanide (HCN) records show a detectable ENSO influence on biomass burning (up to 51%-55%), suggesting that it is wetland CH_4 production that responds less to ENSO than previously suggested. It is possible that other processes obscure the ENSO signal, which itself indicates a minor influence of the latter on CH_4 emissions. Trends like the recent rise in atmospheric [CH_4] can therefore not be attributed to ENSO. This leaves anthropogenic methane sources as the likely driver, which must be mitigated to reduce anthropogenic climate change.

3. Keywords: Time series analyses, isotopes, climate variability, climate change, methane, stable isotope analysis [more]

4. Introduction

Attributing recent changes in the methane budget to specific natural or anthropogenic causes is essential for climate change mitigation. The impact of climatic variability on methane emissions is particularly important to assess the potential for CH_4 release under future climate scenarios (e.g., from permafrost and wetland environments as well as gas hydrates) in a reinforcing feedback. Atmospheric methane mixing ratios [CH_4] have increased by 140% over preindustrial levels (MacFarling Meure et al., 2006). The associated increase in radiative forcing makes CH_4 the second-most important anthropogenic greenhouse gas

Biogeosciences Discuss., https://doi.org/10.5194/bg-2018-304
Manuscript under review for journal Biogeosciences
Discussion started: 24 July 2018

(Shindell et al., 2009). The long-term [CH_4] increase until the late 1990s can be attributed to increasing emissions from fossil fuel production (Ferretti et al., 2005; Schaefer et al., 2016), as well as sources from agriculture (enteric fermentation in livestock, rice production), waste management and anthropogenic burning (van Aardenne et al., 2001; Saunois et al., 2016). After a plateau in the early 2000s, [CH_4] has been rising again since 2007. The signature of stable carbon isotopes in atmospheric methane ($\delta^{13}CH_4$) is influenced by the relative source contributions from ^{13}C-depleted biogenic, ^{13}C-rich pyrogenic, and thermogenic methane with intermediate $\delta^{13}C$. Studies show that biogenic methane sources make either a dominant (Schaefer et al., 2016; Nisbet et al., 2016) or a strong (Worden et al., 2017) contribution to the recent [CH_4] rise. Biogenic methane comes predominantly from wetlands and agriculture. Schaefer et al, (2016) suggested agriculture as the more likely cause, primarily because satellite data place the increased emissions in Southeast Asia, India and China (Houweling et al., 2014). However, this geographic footprint from an inversion of satellite data is also consistent with fluxes from one particular wetland emissions model (Houweling et al., 2014). Other studies also assume a stronger role of wetlands due to drier conditions during the plateau years (Bousquet et al., 2006) and higher wetland emissions afterwards, which are attributed to a switch to predominant La Niña conditions around 2007 (Bousquet et al., 2011; Nisbet et al., 2016). La Niña is the cold phase of El Niño – Southern Oscillation (ENSO) cycles, which have a strong impact on precipitation anomalies in tropical regions (Ropelewski and Halpert, 1987; Lyon and Barnston, 2005) (Fig.1) that are key source areas for methane production from wetlands and biomass burning (Kirschke et al., 2013). ENSO impacts are strongest in the tropics, generally from December to February. During El Niño (La Niña) events in the December to February period, it tends to be drier (wetter) in the Indonesian region, north-east Brazil and south-eastern Africa, whereas it tends to be wetter (drier) in the southern USA and Mexico, eastern China and Taiwan, and east-central Africa (Fig. 1). During El Niño (La Niña) events in the June to August period, it tends to be drier (wetter) in the Indonesian region, central America and India.

The generally drier conditions during an El Niño phase suppress global wetland emissions in models by up to 19 Tg/yr in the 1990s (Hodson et al., 2011). At the same time, dry El Niño phases enhance CH_4 emissions from both natural and anthropogenic biomass burning (van der Werf et al., 2006). Wet La Niña conditions have the opposite effect; summed across the globe they increase wetland emissions and lower biomass burning CH_4. As tropical wetland fluxes are considerably larger than biomass burning emissions (Saunois et al., 2017), the expected net effect is a lower [CH_4] growth rate caused by El Niño conditions and a higher one due to La Niñas. The ENSO impact on $\delta^{13}CH_4$ should be more pronounced than the one on [CH_4], because changes in wetland and biomass burning emissions combine to deplete atmospheric CH_4 in ^{13}C during El Niños and enrich it during La Niñas. Biogenic methanogenesis in wetlands discriminates strongly against ^{13}C and creates methane that is ^{13}C-depleted ($\delta^{13}C$ = -58‰ for tropical wetlands) relative to the plant precursor material ($\delta^{13}C$ of -12‰ to -28‰) and to the aggregate source ($\delta^{13}C$ ~ -53.5‰). In contrast, during burning the isotope ratios of the precursor plant material are essentially conserved and lead to $\delta^{13}C$ ~ -22‰ for CH_4 emissions from fires (Schwietzke et al., 2016). The simultaneous suppression of ^{13}C-depleted wetland CH_4 and enhancement of very ^{13}C-rich pyrogenic emissions (and vice versa) act in the same direction on the $\delta^{13}CH_4$ of the combined source. The latter should be detectable in atmospheric $\delta^{13}CH_4$ records if the impact of ENSO on

the CH_4 cycle is sufficiently large, as is predicted by the emission anomalies in wetland emission models (Hodson et al., 2011), reconstructed from satellite observations of burned area (van der Werf et al., 2010), and observed through variability in hydrogen cyanide (HCN) (Pumphrey et al., 2018), which is an indicator of biomass burning.

We conduct correlation analyses between ENSO variability and [CH_4], as well as $\delta^{13}CH_4$ records to quantify the strength of the impact of ENSO on the CH_4 cycle. Specifically, we explore how much of the year-to-year variability in the methane budget can be attributed to ENSO and how large the ENSO-CH_4 signal is in dependence of latitude. We test if recent trends in methane growth rate can be attributed to wetland emissions controlled by ENSO dynamics or if agricultural sources are more likely drivers. ENSO is quantified by four different indices, which are based on ocean temperature, sea level pressure gradients and a multivariate combination. [CH_4] and $\delta^{13}CH_4$ time series from four different locations were used, two from stations in the Southern tropics (Samoa, SMO, and Ascension Island, ASC), the Southern mid-latitudes (Baring Head, NZ; BHD) taken as representative of the Southern hemisphere, and global average time series of [CH_4] and $\delta^{13}CH_4$ calculated from a network of global stations (Dlugokencky et al., 2011; Schaefer et al., 2016). We also investigate ENSO's impact on HCN data measured in Lauder, NZ (LAU), to quantify the biomass burning contribution separately. The aim is to detect the impact of ENSO on the CH_4 budget on various spatial scales.

5.1. Methods

5.1.1. Data

For access to all data sets used in this study see Sect. 10

5.1.1.1. ENSO indices

We used four different indices in our analysis to cover various climatic effects of the ENSO cycle (Figs. 2A and 3A). The Southern Oscillation Index (SOI) is calculated from the gradient in mean sea-level pressure observations at Tahiti and Darwin, Australia (Troup, 1965). Further information on the SOI is given by (Horel and Wallace, 1981; Trenberth, 1976). The Ocean Niño Index (ONI) uses sea surface temperature (SST) anomalies in the eastern Pacific Niño 3.4. region (5°N-5°S, 120-170°W), which show smaller intra-seasonal variability than pressure and are further smoothed by using 3-month running means (Barnston et al., 1997; Kousky and Higgins, 2007).

The El Niño Modoki Index (EMI) is based on SST anomalies in the central Pacific (Ashok et al., 2007) rather than the eastern Pacific (the canonical El Niño). Events with the largest SST anomalies in the Modoki region show differences in the climate teleconnections to canonical El Niño events. The tropical precipitation differences are modest, but large differences in tropospheric circulation and wind anomalies (Yeh et al., 2009) can produce large extra-tropical differences in precipitation and temperature. The EMI has also been shown to be a significant predictor of tropical atmospheric ozone variations (Xie et al., 2014).

Variability in both atmospheric pressure and SST anomalies informs the Multivariate ENSO Index (MEI) (Wolter and Timlin, 1993; Wolter and Timlin, 1998). The various indices correlate highly with each other (r^2 = 0.85 and higher), except the EMI (r^2 between 0.33 and 0.52 for correlations with SOI, ONI and MEI), which deviates from the others during the strong 1997-198 El Niño event. Excluding the latter brings the correlation to r^2 between 0.74 and 0.79.

An ENSO index based on precipitation data, the ESPI, (Curtis and Adler, 2000) correlates very highly with the MEI, the ONI, and the SOI (r^2 of 0.902, 0.909, and 0.839, respectively). Therefore, we did not conduct separate calculations for the ESPI.

5.1.1.2. [CH_4] time series

The [CH_4] time series used in this study are from the Global Monitoring Division of the National Oceanic and Atmospheric Administration - Earth System Research Laboratory (NOAA ESRL) Carbon Cycle Cooperative Global Air Sampling Network (Dlugokencky et al., 2017). These data include records from SMO (latitude 14.24^{0}S, longitude 170.57^{0}W) and ASC (7.92^{0}S, 14.42^{0}W) as well as global averages calculated by smoothing background data temporally and zonally; all with coverage from 1983-2017. In addition, we use data measured at the NZ National Institute of Water and Atmospheric Research (NIWA) from BHD in NZ (41.41^{0}S, 174.87^{0}E; 1992-2017). The individual time series (Figs. 2B-E) show seasonal cycles, inter-annual variability (IAV) and long-term trends. To investigate ENSO effects on these different time scales we derived the following seven records from the individual measurements at each station. First, the nominal monthly mean values to capture the full variability in the data ("nom"). Second, 12-month running means to represent IAV and trends ("run"). Third, monthly resolved growth rate defined as the difference between the following 12 months and the preceding 12 months ("gro"). Fourth, a residual ("res") as calculated by seasonal trend analysis by Loess (STL, Cleveland et al., 1990). The seasonal window was set at 120 months, which forces a uniform seasonal cycle over the duration of the record. The residual therefore represents IAV in the expression of the seasonal cycle as well as other short-term anomalies. Fifth, sixth, and seventh: detrended time series where the STL trend component is subtracted from the monthly means with subsequent determination of detrended monthly means, 12-month running means, and growth rate ("det-nom", "det-run", "det-gro").

5.1.1.3. $\delta^{13}CH_4$ time series

The $\delta^{13}CH_4$ time series used in this study were measured at three different laboratories, i.e., the Institute of Arctic and Alpine Research (INSTAAR), USA, the Institute for Environmental Physics (IUP) at Heidelberg University, Germany and at NIWA. Details of the analytical methods are given by Schaefer et al. (2016) and references therein. All values are based on measured ^{13}C /^{12}C ratios and are reported in the standard δ-notation $\delta^{13}C = (R_{sample}/R_{standard}-1)*1000‰$ as per mille (‰) values where the

reference standard is Vienna PeeDee Belemnite. Records at SMO (1998-2016) and ASC (2000-2016) are measured at INSTAAR. The BHD record (1992-2016) is based on measurements at INSTAAR and NIWA. An annually averaged global $\delta^{13}CH_4$ time series was established by Schaefer et al. (2016) based on data from INSTAAR, NIWA and IUP. In this analysis, we use the measurements covering 1992-2016 (Fig. 3C). For the global $\delta^{13}CH_4$ data set we conducted the analysis for the nominal annual means ("nom") and growth rate, i.e. difference between two subsequent yearly values ("gro"). We also detrended the time series by subtracting linear trends for the sub-periods 1992-1999 and 2007-2016 ("det") and then calculated a detrended growth rate ("det-gro"). For the single-station $\delta^{13}CH_4$ records of BHD, ASC, and SMO we derived the same seven records as described for the $[CH_4]$ data (Fig. 3D-F).

5.1.1.4. HCN time series

HCN retrievals were computed from mid-infrared solar spectra measured at LAU (45.04°S, 169.68°E) as part of the Network for the Detection for Atmospheric Composition Change (NDACC). The time series has been described by Zeng et al. (2012), but the data used here are from updated retrievals using the improved SFIT4 algorithm (NDACC, 2014). The HCN data show strong seasonality that is even more pronounced in the updated retrievals. Zeng et al. (2012) found a significant negative trend for 1997-2009 and attributed it to variations in biomass burning. A similar deseasonalised trend is apparent in the updated record. HCN values are here reported as Petamolecules cm^{-2}. Measurements cover the period 1998-2017 when combined for two different instruments with a change-over point in 2000. We conducted our analyses for total column values (0-100 km). The latter signal is dominated by the tropospheric burden as measured in the 0-12 km height partial column; the correlation between total and tropospheric HCN is $r^2 = 0.997$. In addition, we investigated whether the stratospheric HCN burden is differently impacted by ENSO. To that end, we used the 12-100 km partial column, which holds ~22% of the total HCN burden. This layer shows lower correlation with the total column record ($r^2 = 0.45$).

Analogous to the monthly resolved methane records we constructed monthly means, 12-month running means, growth rates and STL residuals for the total column and stratospheric HCN data (Fig. 3B). No detrended records other than STL residual were considered.

5.1.2. Analysis

We conducted correlation analyses between the time series of a chosen ENSO index and either a $[CH_4]$, $\delta^{13}CH_4$, or HCN record as the dependent variable. The degree of correlation is quantified by the square (r^2-value) of the Pearson correlation coefficient or, alternatively, the Spearman ranking coefficient. The Pearson coefficient is more commonly used, but it assumes linear relationships between the variables and may underestimate nonlinear correlations. We therefore also used the Spearman rank, which does not require linearity. Note that not all correlation combinations were tested using both coefficients.

A lag time between ENSO forcing and detection of resulting $\delta^{13}CH_4$ or HCN variability at the measurement site, (or in the global average) is likely, due to delayed reaction of methanogenesis or burning to environmental changes, as well as

atmospheric transport and mixing between source regions and sampling sites. Literature estimates of such lags range from days (Chamberlain et al., 2016) to 7 months (Zhu et al., 2017), not counting atmospheric transport. Given ENSO variability with a periodicity of 2-7 years (McPhaden et al., 2006), our analysis therefore allows for lag times of up to 5 years in monthly increments in the calculations and reports the maximum r^2 and lag time for a given ENSO-[CH_4]/$\delta^{13}CH_4$/HCN combination. We conducted the analysis for all permutations of the four ENSO indices as monthly means and their 12-month running means as well as the [CH_4], $\delta^{13}CH_4$, and HCN data products listed in Sect. 2.1. For all [CH_4], $\delta^{13}CH_4$, and HCN parameters we used the period 1998-2016, except for ASC where data are available only from late 2000. Using the same period for all time series avoids differing correlation results due to varying data coverage. The period includes the strong El Niños of 1998 and 2015, as well as the strong La Niñas of 1999, 2007 and 2010. We also calculated correlations for the period 1983-2016 ([CH_4] of SMO, ASC and global) and 1992-2016 ($\delta^{13}CH_4$ at BHD and global).

5.2. Results

Most combinations have r^2-values <0.1 when comparing one dependent data set to the different ENSO time series (Tables 1-3). In the following, we only summarise results for the highest r^2 for each dependent time series (across all the nominal, smoothed and detrended records for a station). Given that Pearson coefficient and Spearman rank give comparable results (Tables 2 and 3), we quote the Spearman results unless otherwise mentioned.

Methane mixing ratios show correlations with ENSO of r^2-values up to 0.36 at SMO, but only for detrended time series (Table 1). Here, lag times are fairly consistent across the various ENSO indices and generally shorter than 1 year. For other [CH_4] records at SMO and ASC the correlations are r^2<0.23 with lags of over 3 years. The global running mean [CH_4] time series shows r^2=0.24 (lag: 4.5 years) with the SOI running mean for the period 1998-2016. However, for the full length of available data, as well as all BHD records, all correlations are below r^2=0.2, with lag times that are variable, extremely short (zero or 1 month) or over 3 years.

The highest correlations are between HCN running means for total column, as well as stratospheric growth rates, and 12-month running mean ENSO records (Table 2). Here, ENSO accounts for 30%-51% of the observed variability, depending on the ENSO index. For both total and stratospheric HCN, lag times for maximum correlation are generally shorter than one year and are consistent (≤6 months difference) between the various ENSO indices, with exception of the EMI.

The $\delta^{13}CH_4$ records from the stations SMO, ASC, and BHD all have r^2-values below 0.24 (Table 2). Variability in lag times between different ENSO indices for the same dependent record is generally high.

For the global detrended $\delta^{13}CH_4$, 37% of variability can be attributed to SOI monthly means. Global $\delta^{13}CH_4$, is the only parameter where ENSO monthly means produce higher correlations than the smoothed (12-month running mean) record. Because the correlation calculation between annual $\delta^{13}CH_4$ and ENSO monthly means is specific for the month-of-year, this finding indicates that global $\delta^{13}CH_4$ is more sensitive to the seasonality of ENSO than its IAV. The actual ENSO influence on global $\delta^{13}CH_4$ is shown through correlation with running ENSO indices, which is highest between nominal $\delta^{13}CH_4$ values and SOI with Pearson $r^2 = 0.25$ for 1998-2016. For the period 1992-2016 this value drops to Pearson $r^2 = 0.20$.

The full BHD record for 1992-2016 gives very similar results as the 1998-2016 subset used for comparison with the other stations (as discussed above). However, the shorter subset for 1998-2014 produces larger Pearson r^2-values (0.26 for running means and SOI), and for 2001-2014 we find Pearson r^2-values up to 0.38 (growth rate correlated to EMI). These shorter data sets omit the strong El Niño events of 1998 and/or 2015-16, which could have been expected to have a strong influence on methane emissions and consequently $\delta^{13}CH_4$.

For none of the stations (including global average) did the detrended $\delta^{13}CH_4$ time series (incl. STL residuals) produce a markedly stronger correlation with ENSO than any of the other data series from that station. This is remarkable because ENSO can be expected to have more influence on IAV than on the long-term trends, which are quite pronounced.

5.3. Discussion

5.3.1. General causes and caveats for correlations of $[CH_4]$, $\delta^{13}CH_4$, and HCN with ENSO

Detected correlations between ENSO indices and $[CH_4]/\delta^{13}CH_4$/HCN by themselves do not prove a causal relationship. However, the underlying mechanisms for a potential forcing have been presented by van der Werf et al. (2006) for biomass burning and by Hodson et al. (2011) for wetland CH_4 production. Accordingly, a correlation analysis is useful to quantify an upper limit of variability in the CH_4 cycle attributable to ENSO. Because ENSO simultaneously suppresses wetland CH_4 that is more ^{13}C-depleted than the cumulative methane source and enhances pyrogenic CH_4 that is more ^{13}C-enriched (or vice versa), the two influences partly cancel for the combined emission rates, i.e. their impact on $[CH_4]$. However, they reinforce each other's impact on total source $\delta^{13}CH_4$. It is possible that biomass burning and wetland CH_4 production have different response times to ENSO forcing, which would weaken their cumulative impact on $\delta^{13}CH_4$. Similarly, longer atmospheric residence time of CH_4 (~9 years, Prather et al., 2012) over HCN (~3 months, Li et al., 2000) and a smaller relative portion of ENSO-sensitive emissions in the global methane source may lead to dampening effects in the $[CH_4]$ and $\delta^{13}CH_4$ variability and hence lower correlation with ENSO indices compared to HCN. The available records for HCN and $\delta^{13}CH_4$ from ASC and SMO cover only a small number of ENSO events, which could affect the results. However, when analysing subperiods of global and BHD $[CH_4]$ and $\delta^{13}CH_4$ records, we find larger correlations for shorter periods, particularly when strong ENSO

events are excluded. This shows that the results are not biased against the detection of ENSO influences because records are too short. We also note that all stations measure background air, they are set up to detect broad spatial and temporal trends and not specific emission events such as an ENSO triggered plume. However, if ENSO is invoked as a main cause of recent trends in [CH_4] and $\delta^{13}CH_4$ (Nisbet et al., 2016) this should be manifested in sizeable correlations.

5

5.3.2. Contrasting correlation patterns for [CH_4] and $\delta^{13}CH_4$ versus HCN

In all [CH_4] and $\delta^{13}CH_4$ records, ENSO cycles explain about one third of the variability in detrended records and less than one quarter in others. This is true even for the Southern tropics, where ENSO has strong climatic impacts and where the majority of low-latitude wetland emissions and of biomass burning emissions originate (Kirschke et al., 2013). Correlations found for
10 ASC and SMO, which represent this latitude band in our study, exceed those for the Southern mid-latitudes or the global record only by a limited margin and only for detrended records. Further, inconsistent lag times, lags of more than three years, and higher correlation coefficients for the exclusion of major ENSO events point to spurious correlations.

In contrast, we find a prominent influence of ENSO on the biomass burning proxy HCN. ENSO impacts on HCN have been reported before, e.g., by Pumphrey et al.)2018), who observe suppression of HCN levels during La Niña events and
15 enhancement during El Niños, particularly in equatorial Asia. That study found a rather confined geographical impact of El Niño events with strongly enhanced HCN emissions around Malaysia, Indonesia, and Papua New Guinea, as well as generally rapid transport eastward and to the stratosphere. We speculate that the fast, upward transport (although not observed for all El Niño events) explains why stratosphere growth rates are the most sensitive data set to ENSO. For the total column, the HCN burden is concentrated in lower tropospheric levels and may be subjected to more mixing of different air parcels. According
20 to the results of Pumphrey et al. (2018), data from LAU in the Southern mid-latitudes are outside the region of the strongest HCN signal. This is also evident in the zonal mean HCN climatologies of (Sheese et al., 2017). Yet, ENSO accounts for up to 51% of the variability in our biomass burning proxy record. That the combined wetland-pyrogenic $\delta^{13}CH_4$ signal is lower suggests that either the sensitivity of wetland CH_4 production to ENSO events is low, or that other processes in the CH_4-cycle obscure the ENSO impacts.

25

5.3.3. Impact of ENSO on methane emission rates

In a correlation analysis by Zhu et al. (2017), ENSO explained 49% of IAV in modelled tropical wetland CH_4 emissions. This is far higher than the combined effect with biomass burning on $\delta^{13}CH_4$ in this study and therefore seems to be an overestimate. Even so, the magnitude of the modelled emission changes is 6 Tg/yr at most. The modelling study of Hodson
30 et al. (2011) finds slightly larger anomalies in global wetland emissions due to ENSO with mean reductions of -9±3 Tg/yr and mean gains of +8±4 Tg/yr for El Niño and La Niña events, respectively. Pandey et al. (2017) found in a comprehensive inversion study that the net effect of the strong 2011 La Niña on tropical and northern extratropical CH_4 emissions was a global increase of +6.6 Tg/yr. The wetland emission anomalies are expected to be partly compensated by changes in biomass burning that are of opposite sign. We are not aware of studies that quantify biomass burning anomalies for specific ENSO

events. Assuming that ENSO is the main control of biomass burning emissions of CH_4, the IAV in the GFED data (van der Werf et al., 2010) may serve as an indication for possible ENSO impacts. In that case, the standard deviation of 2.4 Tg/yr for 1998-2014 would approximate the average impact, with maximum anomalies of up to 4 Tg/yr. We use these numbers together with results from Hodson et al. (2011) in the following proof-of-concept discussions. The combined wetland – biomass burning anomalies are ~6 Tg/yr for average ENSO events and ~8 Tg/yr for extreme ones; restricted to 1-2 yearlong individual events. This is well short of the sustained increase after 2007 when yearly emissions were ~20 Tg higher than during the 1999-2006 plateau period and the 9 Tg/yr reduction during the 1990s. A previous finding of Zhu et al. (2015), that simulated tropical wetland CH_4 emissions can explain at most 25% of the variation in atmospheric methane growth rates (possibly overestimated for the same reasons as the results of Zhu et al. (2017), see above) therefore agrees with our results that ENSO exerts only a minor control on global CH_4 emissions.

5.3.4. Process based understanding of ENSO impact on wetlands

A major contribution of ENSO to the recent [CH_4] increase is inconsistent with independent assessments of wetland response, as shown above, but our findings do not detect any clear minor contribution of ENSO to [CH_4] and $\delta^{13}CH_4$ timeseries, either. Several reasons may explain the lack of correlation, where we assume that wetlands respond less than proposed. The main ENSO forcing on tropical wetland CH_4 production is thought to be via wetland extent, which is driven by precipitation (Hodson et al., 2011; Holmes et al., 2015; in contrast Zhu et al., 2017, find temperature to be dominant). However, a case study in the Eastern Amazon finds that precipitation changes explain only 21% of wetland CH_4 emission variance during the wet season and 7% over the whole year (Basso et al., 2016). The lack of a direct link between precipitation and wetland CH_4 production is also evident in the large range in output from various wetland models even when forced with the same meteorological conditions (Melton et al., 2013), although the disagreement between models could also be due to an incomplete understanding of influences on the wetland cycle other than precipitation (Turetsky et al., 2014; Bridgham et al., 2013; Parker et al., 2018). A complex response of wetland CH_4 production is not only seen in models, however. The inversion study of Pandey et al. (2017) found a global increase of +6.6 Tg/yr for the strong 2011 La Niña, but a reduction by -6.1 Tg/yr during the 2012 weak La Niña. Similarly, Liu et al. (2017) found that El Niño conditions produced opposing weather forcing and carbon cycle responses between various tropical regions, as well as between the 2011 and 2015 events. Another example of this is flooding in the Amazon region during La Niña events, while flooding in the wetlands of the Paraná region occurs during El Niños (Parker et al., 2018). Depending on the strength and geographical expression of the climate anomaly, ENSO may thus cause regional or global emission anomalies that are opposite to the expected pattern.

5.3.5. Evaluating the consistency of ENSO impacts throughout the record

The atmospheric [CH_4] history shows global emission reductions in the 1990s and increases after 2007 (Schaefer et al., 2016). This would be consistent with ENSO forcing of the methane cycle where the 1990s were dominated by drier El- Niño periods, whereas the recent years of predominant La Niña conditions were wetter. Given that the magnitude of the low-latitude wetland

CH_4 source exceeds pyrogenic emissions rates, the expected emissions history would qualitatively match atmospheric trends. Also, for a short period between 2008 and 2011 Schaefer et al. (2016) observed the activation of CH_4 emissions with an extremely ^{13}C-depleted cumulative $\delta^{13}CH_4$ (~-75‰). Such a value on the global scale is hard to match by a single source type. The cumulative effect of wetland enhancement and fire suppression forced by the 2008 La Niña event would provide an excellent explanation. However, the isotopic signal of the emissions reductions in the 1990s should be similar if ENSO forcing was the cause. In contrast, Schaefer et al. (2016) found that the "lost emissions" during that period are quite ^{13}C-rich and rather indicate a reduction in fossil fuel methane. An alternative interpretation of these isotope trends by Rice et al. (2016) requires simultaneous reductions of pyrogenic and biogenic emissions, which is also inconsistent with the expected ENSO forcing. A consistent match between ENSO phases and global $\delta^{13}CH_4$ is therefore neither evident in the dominant $\delta^{13}CH_4$ trends nor in the correlation analysis presented in this study.

5.3.6. Using isotopes to attribute emission changes

The impact of an ENSO emissions "perturbation" (i.e. the combined emissions anomaly of an event) on atmospheric $\delta^{13}CH_4$ can be assessed in isotope mass balance calculations according to:

$$S_{total}*\delta_{total} = S_1*\delta_1 + S_2*\delta_{2+} S_3*\delta_3 \quad (1)$$

Where, for a given source, S and δ represent emission rate and $\delta^{13}CH_4$, respectively (note that for scenarios discussed here S may be negative, i.e., a reduction in emissions). Using generic isotope source signatures for biogenic, fossil fuel and pyrogenic methane emissions from Schwietzke et al. (2016), we find that the average La Niña perturbations proposed in section 4.3. have an effective $\delta^{13}CH_4$ of -79‰, with -83‰ for extreme ones. As expected, the combined isotope leverage of wetland enhancement and fire reductions on the global source is strong, equalling the leverage of much larger source anomalies (20 Tg/yr) with lower $\delta^{13}CH_4$ of ~-60‰ after 2007 as calculated by Schaefer et al. (2016). In addition to the assumed 6 Tg/yr ENSO perturbation, another ~14 Tg/yr of emissions with $\delta^{13}CH_4$=-52‰ would be necessary to produce the observed [CH_4] and $\delta^{13}CH_4$ trends. The isotope mass balance then shows that the non-ENSO additional emissions are a roughly equal mix of fossil fuel and biogenic methane. Noting that the assumption that all years after 2007 experienced average La Niña conditions is unrealistic, these findings therefore show conservatively the following three points: (i) ENSO effects alone cannot explain the post-2007 [CH_4]-rise. (ii) There was an increase in other biogenic sources in addition to ENSO driven wetland emissions. In the absence of boreal emission increases (Sweeney et al., 2016), the only biogenic source that is large enough to accommodate such changes is agriculture (Saunois et al., 2016). (iii) Any ENSO-driven reduction in biomass burning after 2007 allows for, or requires, growing fossil fuel emissions. The latter has recently been proposed by Worden et al. (2017), who reconstructed larger biomass burning reductions after 2007 than recorded by GFED, although without assigning the reductions to ENSO or other causes.

5.3.7. Role of other methane cycle processes

There is an alternative explanation for the lack of correlation between ENSO and the methane records. ENSO could affect CH_4 emissions from tropical wetlands and biomass burning as predicted by Hodson et al. (2011) and van der Werf et al. (2006), respectively, but the resulting isotopic signal is overwhelmed by other components of the CH_4 cycle. Such influences could be other sources (particularly anthropogenic ones), variability in atmospheric transport or changes in CH_4 sink processes. A stronger ENSO signal in Southern tropical [CH_4] and $\delta^{13}CH_4$ compared to Southern mid-latitudes and global average would be expected in this scenario. This is because both biomass burning and wetland emissions show strong maxima in the Southern tropics and should be the dominant sources in this latitudinal band (Kirschke et al., 2013). The detrended [CH_4] records from SMO show such a signal, but one that explains only one third of the IAV and doesn't seem to have significant impact on the trends. Further, we don't find higher ENSO forcing of the $\delta^{13}CH_4$ variability even in the core region of its climatic impact. Whether ENSO has less influence on CH_4 emissions than assumed or whether such an impact is overwhelmed by other CH_4 cycle processes, our results suggest that global atmospheric trends in [CH_4] and $\delta^{13}CH_4$ are dominated by other components in the methane budget.

6. Conclusions

To study the impact of natural climate variability on recent trends in atmospheric methane concentration, we investigated the correlation between ENSO cycles and records of the mixing ratios and stable carbon isotopes of methane, as well as HCN as a biomass burning indicator. As $\delta^{13}CH_4$ is subject to a mutually reinforcing signal from ENSO suppression of wetland emissions and enhancement of biomass burning CH_4 (or vice versa) it is particularly suited to study the role of ENSO in the CH_4 cycle.

We find a sizeable effect of ENSO on biomass burning, as indicated by HCN variability in Southern mid-latitudes. In contrast, ENSO explains a smaller fraction (≤37%) of $\delta^{13}CH_4$ IAV even in the Southern tropics, where the expected effect should be greatest. Trends in [CH_4] and $\delta^{13}CH_4$ in these latitudes are far less influenced by ENSO (≤23%). On hemispheric and global scales the ENSO signal in the methane records is similarly weak. Our results do not rule out that ENSO influences CH_4 emissions from wetlands and biomass burning through enhanced precipitation or droughts in key regions, but any such impacts are overwhelmed by other source and sink processes. Our findings suggest that ENSO is not an important driver for recent global trends in methane, including the increase in [CH_4] since 2007. The latter rise must therefore have different causes. Our results cannot rule out that wetland production is a main contributor to the post-2007 [CH_4]-rise if driven by environmental controls other than ENSO. However, causes for a rapid shift in wetland production to match the sudden onset of the concentration rise in 2007 are unclear and a recent study does not find an increase in global wetland CH_4 production between 2000 and 2012 (Poulter et al., 2017). Therefore, we consider increasing anthropogenic sources as the more likely cause of the [CH_4]-rise. There is evidence for additional methane emissions from agriculture (Schaefer et al., 2016) and from fossil fuel

sources (Hausmann et al., 2016) and both may contribute to the current rise in [CH_4] (Worden et al., 2017). Further identification of these emissions is necessary to inform climate change mitigation policies and climate projections.

7. Team list

Hinrich Schaefer[1], Dan Smale[1], Sylvia E. Nichol[1], Tony M. Bromley[1], Ross J. Martin[1], Rowena Moss[1], Sylvia Englund Michel[2], James W. C. White[2]

[1]Climate and Atmosphere Centre, National Institute of Water and Atmospheric Research, Wellington, 6021, New Zealand
[2] Institute of Arctic and Alpine Research, Boulder, CO, USA.

8. Copyright statement

Code availability: Not applicable

Data availability

Raw data for individual stations measured by INSTAAR and NIWA are available from the World Data Centre for Greenhouse Gases http://ds.data.jma.go.jp/gmd/wdcgg/introduction.html; [CH_4] and $\delta^{13}CH_4$ data from NOAA_ESRL and INSTAAR are also available from ftp://aftp.cmdl.noaa.gov/data/trace_gases. Data from Heidelberg University are available from http://www.iup.uni-heidelberg.de/institut/forschung/groups/kk/en/Data_html.
Global $\delta^{13}CH_4$ data products are available on request from the corresponding author.
Lauder MIR-FTIR HCN is publicly available from the NDACC archive:
ftp.cpc.ncep.noaa.gov/ndacc/station/lauder/hdf/ftir

Appendices

Supplement link (will be included by Copernicus)

Author contribution: H.S. designed the study, conducted the correlation analysis and prepared the manuscript. E.D. supplied [CH_4] data. T.M.B., R.J.M., R.M. S. E.M. and J.W.C.W. supplied $\delta^{13}CH_4$ data. D.S. supplied HCN data. S.E.N. conducted data processing and analysis.

14. Acknowledgements

We thank B. Graham, E. Behrens, Brett Mullan and S. Mikaloff Fletcher for helpful discussions and advice. Ed Dlugokencky from NOAA ESRL supplied [CH_4] data This project was supported by NIWA funding under Climate and Atmosphere Research Programme CAAC1804 (2017/18 SCI).

15. Disclaimer

16. References

Ashok, K., Behera, S.K., Rao, S.A., Weng, H.Y. and Yamagata, T.: El Nino Modoki and its possible teleconnection, J. Geophys. Res., 112, 2007.

Barnston, A.G., Chelliah, M. and Goldenberg, S.B.: Documentation of a highly ENSO-related SST region in the equatorial Pacific, Atmos. Ocean, 35, 367-383, 1997.

Basso, L.S., Gatti, L.V., Gloor, M., Miller, J.B., Domingues, L.G., Correia, C.S.C. and Borges, V.F.: Seasonality and interannual variability of CH4 fluxes from the eastern Amazon Basin inferred from atmospheric mole fraction profiles, J. Geophys. Res., 121, 168-184, 2016.

Bousquet, P., Ciais, P., Miller, J.B., Dlugokencky, E.J., Hauglustaine, D.A., Prigent, C., Van der Werf, G.R., Peylin, P., Brunke, E.-G., Carouge, C., Langenfelds, R.L., Lathiere, J., Papa, F., Ramonet, M., Schmidt, M., Steele, L.P., Tyler, S.C. and White, J.: Contribution of anthropogenic and natural sources to atmospheric methane variability, Nature, 443, doi:10.1038, 2006.

Bousquet, P., Ringeval, B., Pison, I., Dlugokencky, E.J., Brunke, E.G., Carouge, C., Chevallier, F., Fortems-Cheiney, A., Frankenberg, C., Hauglustaine, D.A., Krummel, P.B., Langenfelds, R.L., Ramonet, M., Schmidt, M., Steele, L.P., Szopa, S., Yver, C., Viovy, N. and Ciais, P.: Source attribution of the changes in atmospheric methane for 2006-2008, Atmos. Chem. Phys., 11, 3689-3700, 2011.

Bridgham, S.D., Cadillo-Quiroz, H., Keller, J.K. and Zhuang, Q.L.: Methane emissions from wetlands: biogeochemical, microbial, and modeling perspectives from local to global scales, Global Change Biol., 19, 1325-1346, 2013.

Chamberlain, S.D., Gomez-Casanovas, N., Walter, M.T., Boughton, E.H., Bernacchi, C.J., DeLucia, E.H., Groffman, P.M., Keel, E.W. and Sparks, J.P.: Influence of transient flooding on methane fluxes from subtropical pastures, J. Geophys. Res., 121, 965-977, 2016.

Cleveland, R.B., Cleveland, W.S., McRae, J.E. and Terpenning, I.: STL: A seasonal-trend decomposition procedure based on Loess, J. Off. Stat., 6, 1990.

Curtis, S. and Adler, R.: ENSO indices based on patterns of satellite-derived precipitation, J. Climate, 13, 2786-2793, 2000.

Dlugokencky, E.J., Lang, P.M., Crotwell, A.M., Mund, J.W., Crotwell, M.J. and Thoning, K.W.: Atmospheric Methane Dry Air Mole Fractions from the NOAA ESRL Carbon Cycle Cooperative Global Air Sampling Network, 1983-2016, in: Division, N.-E.G.M. (Ed.), Version: 2017-07-28, , Path: ftp://aftp.cmdl.noaa.gov/data/trace_gases/ch4/flask/surface/, 2017

Dlugokencky, E.J., Nisbet, E.G., Fisher, R. and Lowry, D.: Global atmospheric methane: budget, changes and dangers, Phil. Trans. Royal Soc. A, 369, 2058-2072, 2011.

Ferretti, D.F., Miller, J.B., White, J.W.C., Etheridge, D.M., Lassey, K.R., Lowe, D.C., MacFarling Meure, C.M., Dreier, M.F., Trudinger, C.M., van Ommen, T.D. and Langenfelds, R.L.: Unexpected changes to the global methane budget over the past 2000 years, Science, 309, 1714-1717, 2005.

Hausmann, P., Sussmann, R. and Smale, D.: Contribution of oil and natural gas production to renewed increase in atmospheric methane (2007-2014): top-down estimate from ethane and methane column observations, Atmos. Chem. Phys., 16, 3227-3244, 2016.

Hodson, E.L., Poulter, B., Zimmermann, N.E., Prigent, C. and Kaplan, J.O.: The El Nino-Southern Oscillation and wetland methane interannual variability, Geophys. Res. Lett., 38, 2011.

Holmes, M.E., Chanton, J.P., Tfaily, M.M. and Ogram, A.: CO2 and CH4 isotope compositions and production pathways in a tropical peatland, Global Biogeochem. Cy., 29, 1-18, 2015.

Horel, J.D. and Wallace, J.M.: Planetary-Scale Atmospheric Phenomena Associated with the Southern Oscillation, Mon. Weather Rev., 109, 813-829, 1981.

Houweling, S., Krol, M., Bergamaschi, P., Frankenberg, C., Dlugokencky, E.J., Morino, I., Notholt, J., Sherlock, V., Wunch, D., Beck, V., Gerbig, C., Chen, H., Kort, E.A., Rockmann, T. and Aben, I.: A multi-year methane inversion using SCIAMACHY, accounting for systematic errors using TCCON measurements, Atmos. Chem. Phys., 14, 3991-4012, 2014.

Kirschke, S., Bousquet, P., Ciais, P., Saunois, M., Canadell, J.G., Dlugokencky, E.J., Bergamaschi, P., Bergmann, D., Blake, D.R., Bruhwiler, L., Cameron-Smith, P., Castaldi, S., Chevallier, F., Feng, L., Fraser, A., Heimann, M., Hodson, E.L., Houweling, S., Josse, B., Fraser, P.J., Krummel, P.B., Lamarque, J.F., Langenfelds, R.L., Le Quere, C., Naik, V., O'Doherty, S., Palmer, P.I., Pison, I., Plummer, D., Poulter, B., Prinn, R.G., Rigby, M., Ringeval, B., Santini, M., Schmidt, M., Shindell, D.T., Simpson, I.J., Spahni, R., Steele, L.P., Strode, S.A., Sudo, K., Szopa, S., van der Werf, G.R., Voulgarakis, A., van Weele, M., Weiss, R.F., Williams, J.E. and Zeng, G.: Three decades of global methane sources and sinks, Nat. Geosci., 6, 813-823, 2013.

Kousky, V.E. and Higgins, R.W.: An alert classification system for monitoring and assessing the ENSO cycle, Weather Forecast, 22, 353-371, 2007.

Li, Q.B., Jacob, D.J., Bey, I., Yantosca, R.M., Zhao, Y.J., Kondo, Y. and Notholt, J.: Atmospheric hydrogen cyanide (HCN): Biomass burning source, ocean sink? Geophys. Res. Lett., 27, 357-360, 2000.

Liu, J.J., Bowman, K.W., Schimel, D.S., Parazoo, N.C., Jiang, Z., Lee, M., Bloom, A.A., Wunch, D., Frankenberg, C., Sun, Y., O'Dell, C.W., Gurney, K.R., Menemenlis, D., Gierach, M., Crisp, D. and Eldering, A.: Contrasting carbon cycle responses of the tropical continents to the 2015-2016 El Nino, Science, 358, 191-193, 2017.

Lyon, B. and Barnston, A.G.: ENSO and the spatial extent of interannual precipitation extremes in tropical land areas, J. Climate, 18, 5095-5109, 2005.

MacFarling Meure, C., Etheridge, D., Trudinger, C., Steele, P., Langenfelds, R., van Ommen, T., Smith, A. and Elkins, J.: Law Dome CO_2, CH_4 and N_2O ice core records extended to 2000 years BP, Geophys. Res. Lett., 33, 2006.

McPhaden, M.J., Zebiak, S.E. and Glantz, M.H.: ENSO as an integrating concept in Earth science, Science, 314, 1740-1745, 2006.

Melton, J.R., Wania, R., Hodson, E.L., Poulter, B., Ringeval, B., Spahni, R., Bohn, T., Avis, C.A., Beerling, D.J., Chen, G., Eliseev, A.V., Denisov, S.N., Hopcroft, P.O., Lettenmaier, D.P., Riley, W.J., Singarayer, J.S., Subin, Z.M., Tian, H., Zurcher, S., Brovkin, V., van Bodegom, P.M., Kleinen, T., Yu, Z.C. and Kaplan, J.O.: Present state of global wetland extent and wetland methane modelling: conclusions from a model inter-comparison project (WETCHIMP), Biogeosciences, 10, 753-788, 2013.

NDACC, Infrared Working Group: IRWG Uniform Retrieval Parameter Summary, http://www.acom.ucar.edu/irwg/IRWG_Uniform_RP_Summary-3.pdf, 2014

Nisbet, E.G., Dlugokencky, E.J., Manning, M.R., Lowry, D., Fisher, R.E., France, J.L., Michel, S.E., Miller, J.B., White, J.W.C., Vaughn, B., Bousquet, P., Pyle, J.A., Warwick, N.J., Cain, M., Brownlow, R., Zazzeri, G., Lanoiselle, M., Manning, A.C., Gloor, E., Worthy, D.E.J., Brunke, E.G., Labuschagne, C., Wolff, E.W. and Ganesan, A.L.: Rising atmospheric methane: 2007-2014 growth and isotopic shift, Global Biogeochem. Cy., 30, 1356-1370, 2016.

Pandey, S., Houweling, S., Krol, M., Aben, I., Monteil, G., Nechita-Banda, N., Dlugokencky, E.J., Detmers, R., Hasekamp, O., Xu, X.Y., Riley, W.J., Poulter, B., Zhang, Z., McDonald, K.C., White, J.W.C., Bousquet, P. and Rockmann, T.: Enhanced methane emissions from tropical wetlands during the 2011 La Nina, Sci. Rep., 2017.

Parker, R.J., Boesch, H., McNorton, J., Comyn-Platt, E., Gloor, M., Wilson, C., Chipperfield, M.P., Hayman, G.D. and Bloom, A.A.: Evaluating year-to-year anomalies in tropical wetland methane emissions using satellite CH4 observations, Remote Sens. Environ., 211, 261-275, 2018.

Poulter, B., Bousquet, P., Canadell, J.G., Ciais, P., Peregon, A., Saunois, M., Arora, V.K., Beerling, D.J., Brovkin, V., Jones, C.D., Joos, F., Gedney, N., Ito, A., Kleinen, T., Koven, C.D., McDonald, K., Melton, J.R., Peng, C.H., Peng, S.S., Prigent, C., Schroeder, R., Riley, W.J., Saito, M., Spahni, R., Tian, H.Q., Taylor, L., Viovy, N., Wilton, D., Wiltshire, A., Xu, X.Y., Zhang, B.W., Zhang, Z. and Zhu, Q.A.: Global wetland contribution to 2000-2012 atmospheric methane growth rate dynamics, Environ. Res. Lett., 12, 2017.

Prather, M.J., Holmes, C.D. and Hsu, J.: Reactive greenhouse gas scenarios: Systematic exploration of uncertainties and the role of atmospheric chemistry, Geophys. Res. Lett., 39, 2012.

Pumphrey, H.C., Glatthor, N., Bernath, P.F., Boone, C.D., Hannigan, J.W., Ortega, I., Livesey, N.J. and Read, W.G.: MLS measurements of stratospheric hydrogen cyanide during the 2015-2016 El Nino event, Atmos. Chem. Phys., 18, 691-703, 2018.

Rice, A.L., Butenhoff, C.L., Teama, D.G., Roger, F.H., Khalil, M.A.K. and Rasmussen, R.A.: Atmospheric methane isotopic record favors fossil sources flat in 1980s and 1990s with recent increase, Proc. Nat. Acad. Sci. USA, 113, 10791-10796, 2016.

Ropelewski, C.F. and Halpert, M.S.: Global and Regional Scale Precipitation Patterns Associated with the El-Nino Southern Oscillation, Mon. Weather Rev., 115, 1606-1626, 1987.

Saunois, M., Bousquet, P., Poulter, B., Peregon, A., Ciais, P., Canadell, J.G., Dlugokencky, E.J., Etiope, G., Bastviken, D., Houweling, S., Janssens-Maenhout, G., Tubiello, F.N., Castaldi, S., Jackson, R.B., Alexe, M., Arora, V.K., Beerling, D.J., Bergamaschi, P., Blake, D.R., Brailsford, G., Brovkin, V., Bruhwiler, L., Crevoisier, C., Crill, P., Covey, K., Curry, C., Frankenberg, C., Gedney, N., Hoglund-Isaksson, L., Ishizawa, M., Ito, A., Joos, F., Kim, H.S., Kleinen, T., Krummel, P., Lamarque, J.F., Langenfelds, R., Locatelli, R., Machida, T., Maksyutov, S., McDonald, K.C., Marshall, J., Melton, J.R., Morino, I., Naik, V., O'Doherty, S., Parmentier, F.J.W., Patra, P.K., Peng, C.H., Peng, S.S., Peters, G.P., Pison, I., Prigent, C., Prinn, R., Ramonet, M., Riley, W.J., Saito, M., Santini, M., Schroeder, R., Simpson, I.J., Spahni, R., Steele, P., Takizawa, A., Thornton, B.F., Tian, H.Q., Tohjima, Y., Viovy, N., Voulgarakis, A., van Weele, M., van der Werf, G.R., Weiss, R., Wiedinmyer, C., Wilton, D.J., Wiltshire, A., Worthy, D., Wunch, D., Xu, X.Y., Yoshida, Y., Zhang, B., Zhang, Z. and Zhu, Q.: The global methane budget 2000-2012, Earth Syst. Sci. Data, 8, 697-751, 2016.

Saunois, M., Bousquet, P., Poulter, B., Peregon, A., Ciais, P., Canadell, J.G., Dlugokencky, E.J., Etiope, G., Bastviken, D., Houweling, S., Janssens-Maenhout, G., Tubiello, F.N., Castaldi, S., Jackson, R.B., Alexe, M., Arora, V.K., Beerling, D.J., Bergamaschi, P., Blake, D.R., Brailsford, G., Bruhwiler, L., Crevoisier, C., Crill, P., Covey, K., Frankenberg, C., Gedney, N., Hoglund-Isaksson, L., Ishizawa, M., Ito, A., Joos, F., Kim, H.S., Kleinen, T., Krummel, P., Lamarque, J.F., Langenfelds, R.,

Locatelli, R., Machida, T., Maksyutov, S., Melton, J.R., Morino, I., Naik, V., O'Doherty, S., Parmentier, F.J., Patra, P.K., Peng, C.H., Peng, S.S., Peters, G.P., Pison, I., Prinn, R., Ramonet, M., Riley, W.J., Saito, M., Santini, M., Schroeder, R., Simpson, I.J., Spahni, R., Takizawa, A., Thornton, B.F., Tian, H.Q., Tohjima, Y., Viovy, N., Voulgarakis, A., Weiss, R., Wilton, D.J., Wiltshire, A., Worthy, D., Wunch, D., Xu, X.Y., Yoshida, Y., Zhang, B.W., Zhang, Z. and Zhu, Q.A.: Variability and quasi-decadal changes in the methane budget over the period 2000-2012, Atmos. Chem. Phys., 17, 11135-11161, 2017.

Schaefer, H., Fletcher, S.E.M., Veidt, C., Lassey, K.R., Brailsford, G.W., Bromley, T.M., Dlugokencky, E.J., Michel, S.E., Miller, J.B., Levin, I., Lowe, D.C., Martin, R.J., Vaughn, B.H. and White, J.W.C.: A 21st-century shift from fossil-fuel to biogenic methane emissions indicated by (CH4)-C-13, Science, 352, 80-84, 2016.

Schwietzke, S., Sherwood, O.A., Ruhwiler, L.M.P.B., Miller, J.B., Etiope, G., Dlugokencky, E.J., Michel, S.E., Arling, V.A., Vaughn, B.H., White, J.W.C. and Tans, P.P.: Upward revision of global fossil fuel methane emissions based on isotope database, Nature, 538, 88-91, 2016.

Sheese, P.E., Walker, K.A. and Boone, C.D.: A global enhancement of hydrogen cyanide in the lower stratosphere throughout 2016, Geophys. Res. Lett., 2017.

Shindell, D.T., Faluvegi, G., Koch, D.M., Schmidt, G.A., Unger, N. and Bauer, S.E.: Improved Attribution of Climate Forcing to Emissions, Science, 326, 716-718, 2009.

Sweeney, C., Dlugokencky, E., Miller, C.E., Wofsy, S., Karion, A., Dinardo, S., Chang, R.Y.W., Miller, J.B., Bruhwiler, L., Crotwell, A.M., Newberger, T., McKain, K., Stone, R.S., Wolter, S.E., Lang, P.E. and Tans, P.: No significant increase in long-term CH4 emissions on North Slope of Alaska despite significant increase in air temperature, Geophys. Res. Lett., 43, 6604-6611, 2016.

Trenberth, K.E.: Spatial and Temporal Variations of Southern Oscillation. Q J Roy Meteor Soc 102, 639-653.
Troup, A.J. (1965) Southern Oscillation, Quat. J. Roy. Meteor. Soc., 91, 1976.

Turetsky, M.R., Kotowska, A., Bubier, J., Dise, N.B., Crill, P., Hornibrook, E.R.C., Minkkinen, K., Moore, T.R., Myers-Smith, I.H., Nykanen, H., Olefeldt, D., Rinne, J., Saarnio, S., Shurpali, N., Tuittila, E.S., Waddington, J.M., White, J.R., Wickland, K.P. and Wilmking, M.: A synthesis of methane emissions from 71 northern, temperate, and subtropical wetlands, Global Change Biol., 20, 2183-2197, 2014.

van Aardenne, J.A., Dentener, F.J., Olivier, J.G.J., Goldewijk, C.G.M.K. and Lelieveld, J.: A 1 degrees x 1 degrees resolution data set of historical anthropogenic trace gas emissions for the period 1890-1990, Global Biogeochem. Cy., 15, 909-928, 2001.

van der Werf, G.R., Randerson, J.T., Giglio, L., Collatz, G.J., Kasibhatla, P.S. and Arellano, A.F.: Interannual variability in global biomass burning emissions from 1997 to 2004, Atmos. Chem. Phys., 6, 3423-3441, 2006.

van der Werf, G.R., Randerson, J.T., Giglio, L., Collatz, G.J., Mu, M., Kasibhatla, P.S., Morton, D.C., DeFries, R.S., Jin, Y. and van Leeuwen, T.T.: Global fire emissions and the contribution of deforestation, savanna, forest, agricultural, and peat fires (1997-2009), Atmos. Chem. Phys., 10, 11707-11735, 2010.

Wolter, K. and Timlin, M.S.: Monitoring ENSO in COADS with a seasonally adjusted principal component index, Proc. 17th Climate Diagnostics Workshop, 1993.

Wolter, K. and Timlin, M.S.: Measuring the strength of ENSO events: How does 1997/98 rank? Weather, 53, 315-324, 1998.

Worden, J.R., Bloom, A.A., Pandey, S., Jiang, Z., Worden, H.M., Walker, T.W., Houweling, S. and Rockmann, T.: Reduced biomass burning emissions reconcile conflicting estimates of the post-2006 atmospheric methane budget, Nat. Commun., 8, 2017.

Xie, F., Li, J.P., Tian, W.S., Zhang, J.K. and Sun, C.: The relative impacts of El Nino Modoki, canonical El Nino, and QBO on tropical ozone changes since the 1980s, Environ. Res. Lett., 9, 2014.

Yeh, S.W., Kug, J.S., Dewitte, B., Kwon, M.H., Kirtman, B.P. and Jin, F.F.: El Nino in a changing climate, Nature, 462, 511-513, 2009.

Zeng, G., Wood, S.W., Morgenstern, O., Jones, N.B., Robinson, J. and Smale, D.: Trends and variations in CO, C2H6, and HCN in the Southern Hemisphere point to the declining anthropogenic emissions of CO and C2H6, Atmos. Chem. Phys., 12, 7543-7555, 2012.

Zhu, Q., Peng, C., Chen, H., Fang, X., Liu, J., Jiang, H., Yang, Y. and Yang, G.: Estimating global natural wetland methane emissions using process modelling: spatio-temporal patterns and contributions to atmospheric methane fluctuations, Global Ecol. Biogeogr., 24, 959-972, 2015.

Zhu, Q., Peng, C., Ciais, P., Jiang, H., Liu, J., Bousquet, P., Li, S., Chang, J., Fang, X. and Zhou, X.: Inter-annual Variation in Methane Emissions from Tropical Wetlands Triggered by Repeated El Niño Southern Oscillation, Global Change Biol., 2017.

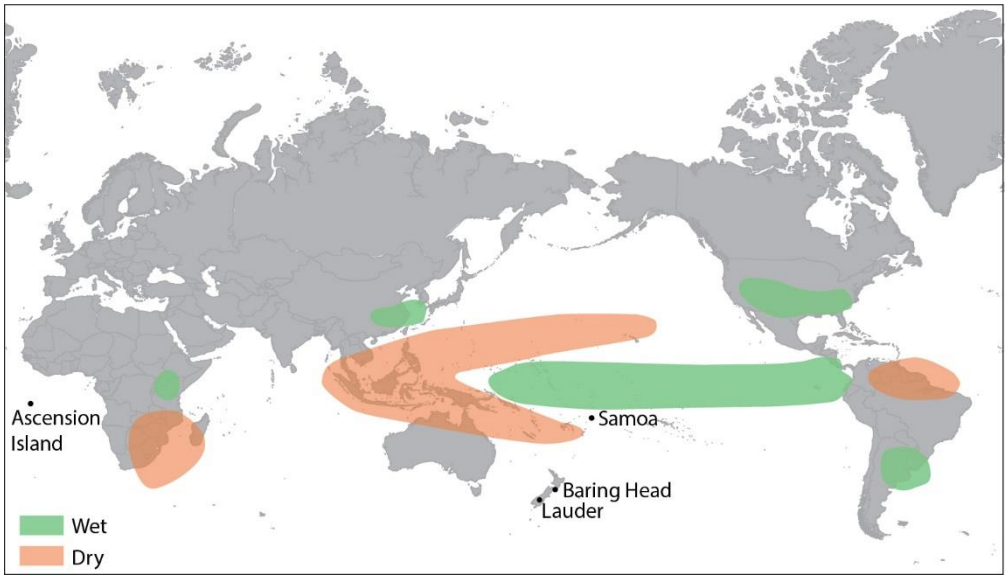

Fig. 1: Regions of ENSO impacts and monitoring stations used in this study.

Biogeosciences Discuss., https://doi.org/10.5194/bg-2018-304
Manuscript under review for journal Biogeosciences
Discussion started: 24 July 2018

The map indicates the locations of the atmospheric monitoring stations on Ascension Island (ASC), Samoa (SMO), Baring Head (BHD) and Lauder (LAU). General precipitation anomalies during northern hemisphere El Niño conditions for Dec-Feb are taken from https://www.climate.gov/news-features/featured-images/global-impacts-el-nino-and-la-nina. El Niño dry regions in Jun-Aug are similar for southern Asia and South America; during La Niña events opposite patterns for wet- and dryness develop in roughly the same regions.

Biogeosciences Discuss., https://doi.org/10.5194/bg-2018-304
Manuscript under review for journal Biogeosciences
Discussion started: 24 July 2018

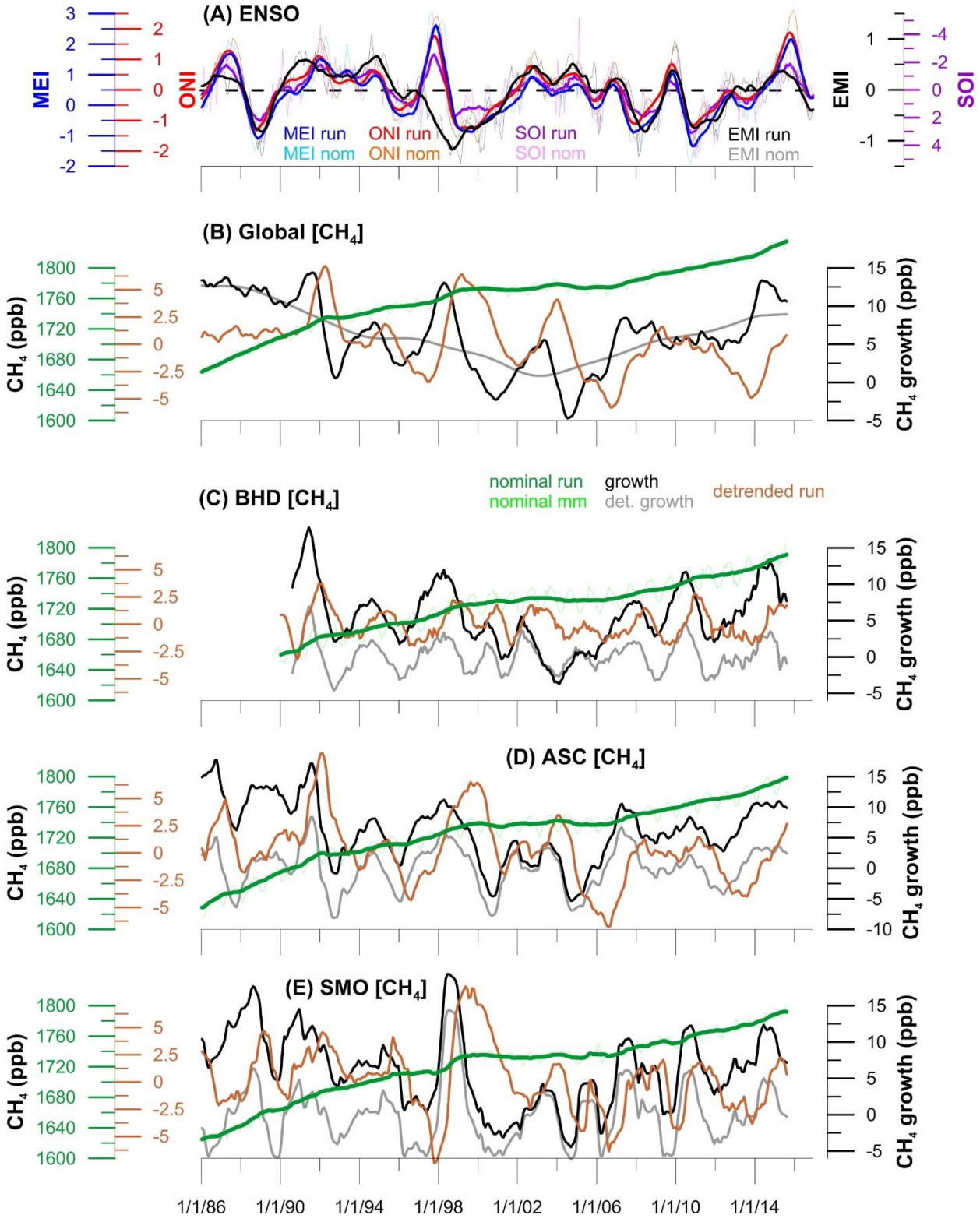

Biogeosciences Discuss., https://doi.org/10.5194/bg-2018-304
Manuscript under review for journal Biogeosciences
Discussion started: 24 July 2018

Fig. 2: Selected time series of ENSO indices and [CH_4]

Panels from top to bottom: (A) multivariate ENSO Index (MEI), Southern Oscillation Index (SOI), Ocean Niño Index (ONI), and El Modoki Index (EMI) shown for nominal literature data and their 12-month running means. (B) Global [CH_4] records; monthly means, 12-month running mean, detrended 12-month running mean, as well as nominal and detrended growth rates. (C) [CH_4] records from BHD (D) [CH_4] records from ASC. (E) [CH_4] records from SMO. BHD, ASC and SMO display same records as for global time series.

Biogeosciences Discuss., https://doi.org/10.5194/bg-2018-304
Manuscript under review for journal Biogeosciences
Discussion started: 24 July 2018

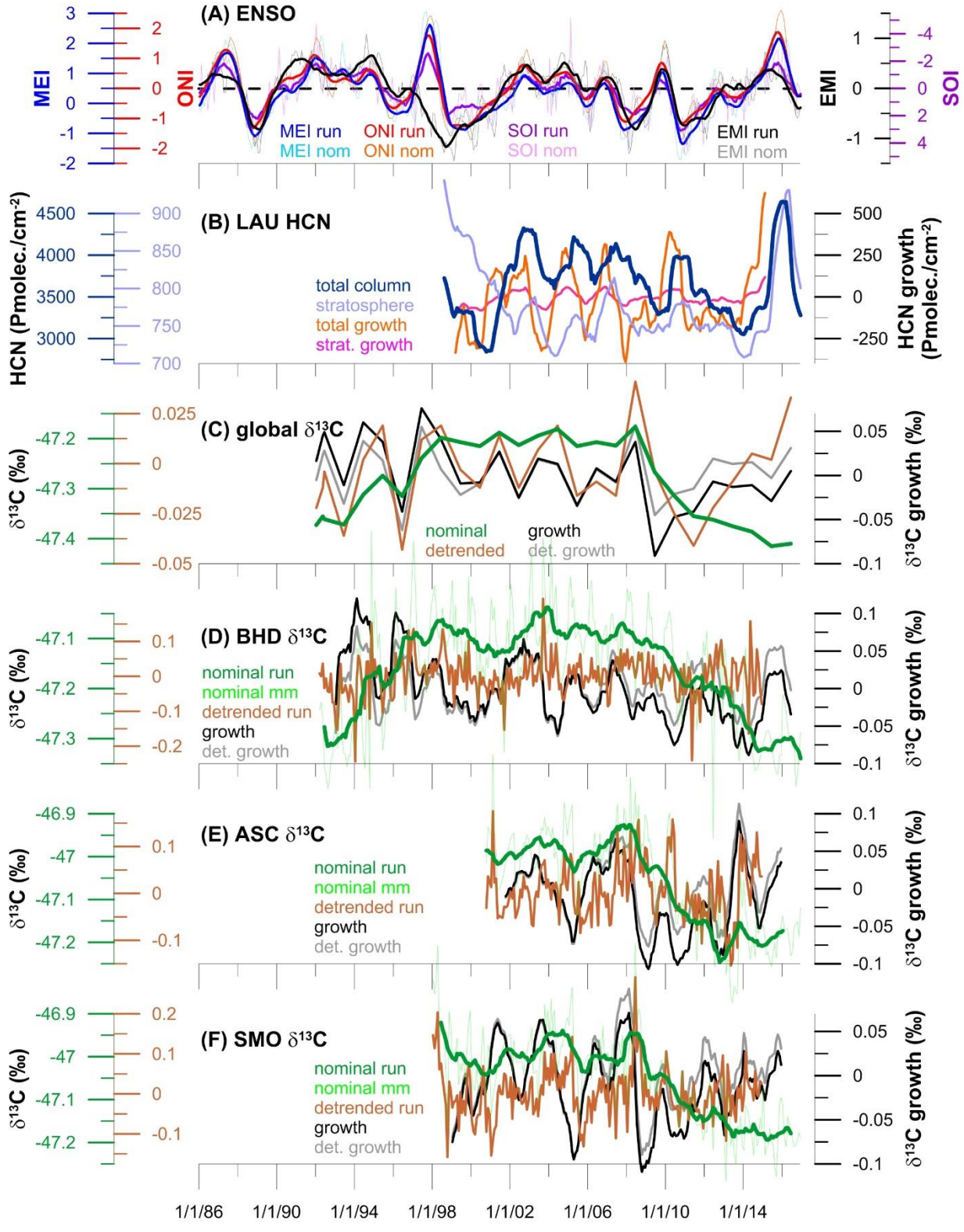

Biogeosciences Discuss., https://doi.org/10.5194/bg-2018-304
Manuscript under review for journal Biogeosciences
Discussion started: 24 July 2018

Fig. 3: Selected time series of ENSO indices, HCN and $\delta^{13}CH_4$

Panels from top to bottom: (A) multivariate ENSO Index (MEI), Southern Oscillation Index (SOI), Ocean Niño Index (ONI), and El Modoki Index (EMI) shown for nominal literature data and their 12-month running means. (B) HCN records as 12-month running means from LAU for total atmospheric column and stratosphere (12-100 km) and respective growth rates. (C) Global annually averaged $\delta^{13}CH_4$ according to Schaefer et al. (2016) updated to end of 2016; nominal and detrended values and their respective growth rates. (D) $\delta^{13}CH_4$ from BHD; monthly means, 12-month running mean, detrended 12-month running mean, as well as nominal and detrended growth rates. (E) $\delta^{13}CH_4$ from ASC. (F) $\delta^{13}CH_4$ from SMO. ASC and SMO display same records as for BHD. Note scale differences between all $\delta^{13}C$-axes to accentuate variability for comparison with ENSO.

Biogeosciences Discuss., https://doi.org/10.5194/bg-2018-304
Manuscript under review for journal Biogeosciences
Discussion started: 24 July 2018

Table 1: Spearman correlation of methane mixing ratio with ENSO variability.

Correlations (r^2-values) for the Spearman ranking coefficient between [CH_4] time series from various sites and ENSO indices with lag times for optimum results. Colour backgrounds indicate r^2-values in 10% classes.

Time series	MEI nom		MEI run		ONI nom		ONI run		SOI nom		SOI run		EMI nom		EMI run	
	r^2	lag	r^2	lag	r^2	lag	r^2	lag	r^2	lag	r^2	lag	r^2	lag	r^2	lag
[CH_4]																
global nom	0.08	59	0.12	58	0.04	48	0.06	50	0.10	59	0.17	54	0.04	5	0.03	10
global gro	0.10	6	0.10	6	0.08	7	0.09	59	0.06	8	0.08	33	0.06	50	0.09	52
global run	0.10	56	0.18	53	0.06	55	0.09	51	0.11	57	0.24	54	0.07	8	0.08	10
global res	0.06	49	0.06	47	0.09	49	0.11	48	0.04	25	0.06	60	0.10	0	0.09	0
global det-nom	0.10	49	0.02	49	0.06	49	0.04	50	0.05	29	0.02	60	0.07	9	0.03	5
global det-gro	0.02	58	0.04	60	0.00	58	0.00	59	0.02	59	0.06	60	0.03	0	0.04	0
global det-run	0.05	49	0.06	48	0.09	48	0.12	49	0.03	0	0.04	60	0.08	0	0.08	1
BHD nom	0.10	56	0.11	58	0.05	45	0.05	47	0.11	56	0.15	59	0.07	53	0.05	51
BHD gro	0.08	24	0.10	27	0.10	51	0.11	55	0.08	24	0.12	24	0.15	60	0.19	60
BHD run	0.05	44	0.11	44	0.04	0	0.07	0	0.08	45	0.17	53	0.08	7	0.09	7
BHD res	0.03	46	0.02	16	0.02	16	0.02	16	0.02	16	0.02	14	0.02	33	0.02	29
BHD det-nom	0.07	44	0.01	17	0.02	33	0.01	36	0.03	13	0.01	17	0.04	30.00	0.00	29
BHD det-gro	0.13	56	0.17	58	0.12	23	0.13	59	0.10	23	0.14	59	0.08	60	0.08	24
BHD det-run	0.10	60	0.14	60	0.07	44	0.09	42	0.07	60	0.11	60	0.08	33	0.11	32
ASC nom	0.09	56	0.11	45	0.05	44	0.06	46	0.10	42	0.16	46	0.05	53	0.04	50
ASC gro	0.09	29	0.13	31	0.11	53	0.13	55	0.06	31	0.11	32	0.15	50	0.21	53
ASC run	0.08	43	0.16	45	0.07	44	0.10	44	0.11	43	0.22	43	0.06	46	0.06	47
ASC res	0.08	42	0.09	18	0.12	42	0.12	42	0.06	41	0.06	60	0.08	0	0.07	2
ASC det-nom	0.11	43	0.02	45	0.06	43	0.03	45	0.06	43	0.01	44	0.06	4	0.02	2
ASC det-gro	0.20	10	0.26	10	0.18	10	0.21	11	0.14	10	0.20	10	0.09	51	0.12	53
ASC det-run	0.09	40	0.14	17	0.13	41	0.15	42	0.05	17	0.08	17	0.09	0	0.08	1
SMO nom	0.07	56	0.12	58	0.03	45	0.04	48	0.08	56	0.16	59	0.02	10	0.02	50
SMO gro	0.19	17	0.18	10	0.15	10	0.17	11	0.10	9	0.12	10	0.13	46	0.17	49
SMO run	0.07	51	0.14	53	0.04	49	0.05	51	0.08	53	0.18	55	0.01	7	0.01	10
SMO res	0.16	0	0.13	1	0.22	1	0.15	1	0.14	0	0.15	2	0.17	0	0.14	3
SMO det-nom	0.15	0	0.11	1	0.18	0	0.14	1	0.09	0	0.12	2	0.10	0	0.11	3
SMO det-gro	0.31	9	0.36	10	0.31	10	0.35	11	0.22	9	0.33	11	0.10	10	0.11	12
SMO det-run	0.26	1	0.24	2	0.29	2	0.27	3	0.21	2	0.25	2	0.23	2	0.21	4

Biogeosciences Discuss., https://doi.org/10.5194/bg-2018-304
Manuscript under review for journal Biogeosciences
Discussion started: 24 July 2018

Table 2: Spearman correlation of $\delta^{13}CH_4$ and HCN with ENSO variability.

Correlations (r^2-values) for the Spearman ranking coefficient between dependent variables, i.e. $\delta^{13}CH_4$ and HCN time series from various sites, and ENSO indices with lag times for optimum results. Colour backgrounds indicate r^2-values in 10% classes.

Time series	MEI nom		MEI run		ONI nom		ONI run		SOI nom		SOI run		EMI nom		EMI run	
	r^2	lag	r^2	lag	r^2	lag	r^2	lag	r^2	lag	r^2	lag	r^2	lag	r^2	lag
HCN (LAU)																
total nom	0.13	5	0.03	6	0.06	5	0.05	8	0.08	4	0.04	8	0.10	14	0.05	12
total gro	0.21	1	0.26	2	0.27	1	0.27	2	0.18	0	0.30	1	0.19	0	0.27	1
total run	0.23	7	0.30	9	0.35	7	0.39	9	0.23	8	0.38	8	0.40	9	0.51	10
total res	0.10	7	0.09	7	0.13	7	0.13	7	0.10	10	0.13	6	0.08	9	0.10	10
strat. nom	0.10	10	0.05	11	0.05	41	0.03	0	0.08	40	0.05	43	0.09	39	0.08	0
strat. gro	0.36	0	0.43	0	0.40	0	0.44	1	0.22	0	0.37	0	0.21	0	0.30	0
strat. run	0.03	37	0.05	38	0.05	0	0.08	0	0.05	40	0.08	41	0.07	18	0.10	0
strat. res	0.10	7	0.07	7	0.10	7	0.08	8	0.07	8	0.07	8	0.11	44	0.10	38
$\delta^{13}CH_4$																
global nom	0.17	2	0.17	49	0.13	2	0.12	50	0.27	46	0.27	49	0.16	4	0.05	47
global gro	0.20	39	0.18	41	0.18	39	0.16	41	0.34	49	0.20	15	0.15	4	0.08	16
global det	0.14	1	0.19	14	0.08	20	0.12	16	0.37	22	0.27	17	0.13	15	0.12	16
global det-gro	0.23	58	0.16	58	0.18	59	0.18	60	0.37	55	0.24	56	0.15	15	0.12	16
BHD nom	0.09	56	0.09	60	0.04	56	0.04	59	0.09	55	0.13	60	0.07	42	0.06	39
BHD gro	0.05	2	0.06	2	0.06	2	0.07	3	0.08	2	0.13	2	0.10	44	0.11	44
BHD run	0.09	14	0.14	16	0.11	15	0.15	17	0.10	15	0.20	17	0.07	29	0.09	36
BHD res	0.03	6	0.03	10	0.04	7	0.03	9	0.04	6	0.03	10	0.09	33	0.09	36
BHD det-nom	0.07	8	0.01	8	0.03	7	0.02	9	0.05	6	0.01	10	0.06	42	0.05	38
BHD det-gro	0.07	1	0.09	1	0.09	1	0.11	2	0.09	2	0.13	12	0.10	45	0.11	45
BHD det-run	0.07	9	0.09	11	0.08	12	0.10	12	0.06	9	0.09	13	0.15	32	0.20	35
ASC nom	0.08	54	0.08	44	0.05	54	0.04	45	0.08	55	0.13	45	0.05	52	0.03	49
ASC gro	0.10	13	0.14	13	0.10	13	0.09	13	0.11	12	0.22	12	0.13	9	0.13	7
ASC run	0.08	22	0.13	23	0.08	22	0.10	22	0.12	22	0.23	22	0.12	20	0.14	20
ASC res	0.03	17	0.04	21	0.03	16	0.02	19	0.05	18	0.06	20	0.03	14	0.03	19
ASC det-nom	0.05	18	0.03	22	0.03	17	0.01	19	0.06	18	0.04	17	0.05	14	0.01	16
ASC det-gro	0.07	13	0.07	14	0.05	13	0.05	60	0.06	12	0.11	13	0.07	8	0.05	6
ASC det-run	0.04	22	0.05	60	0.04	60	0.04	60	0.07	22	0.09	22	0.06	32	0.06	32
SMO nom	0.06	56	0.08	55	0.04	43	0.04	44	0.08	56	0.12	42	0.04	40	0.05	38

Biogeosciences Discuss., https://doi.org/10.5194/bg-2018-304
Manuscript under review for journal Biogeosciences
Discussion started: 24 July 2018

SMO gro	0.02	13	0.03	24	0.02	23	0.03	25	0.04	0	0.06	13	0.10	43	0.10	44
SMO run	0.07	15	0.12	18	0.08	16	0.10	19	0.09	16	0.19	20	0.06	19	0.07	21
SMO res	0.09	0	0.08	0	0.10	1	0.08	2	0.09	1	0.07	3	0.06	30	0.06	35
SMO det-nom	0.06	0	0.06	1	0.08	1	0.06	1	0.06	3	0.05	3	0.06	30	0.05	35
SMO det-gro	0.05	23	0.06	24	0.04	23	0.06	25	0.03	0	0.03	0	0.09	42	0.08	42
SMO det-run	0.17	1	0.20	1	0.20	2	0.22	2	0.12	4	0.16	3	0.13	26	0.14	30

Table 3: Pearson correlation of $\delta^{13}CH_4$ and HCN with ENSO variability.

Correlations (r^2-values) for the Pearson correlation coefficient between dependent variables, i.e. $\delta^{13}CH_4$ and HCN time series from various sites, and ENSO indices with lag times for optimum results. Colour backgrounds indicate r^2-values in 10% classes.

Time series	MEI nom		MEI run		ONI nom		ONI run		SOI nom		SOI run		EMI nom		EMI run	
	r^2	lag	r^2	lag	r^2	lag	r^2	lag	r^2	lag	r^2	lag	r^2	lag	r^2	lag
HCN (LAU)																
total nom	0.10	5	0.03	5	0.04	4	0.04	6	0.06	4	0.04	6	0.10	14	0.06	11
total gro	0.22	0	0.30	2	0.27	1	0.30	1	0.16	0	0.28	2	0.19	2	0.24	1
total run	0.22	4	0.29	6	0.34	6	0.40	7	0.18	6	0.34	8	0.36	10	0.46	11
total res	0.11	7	0.13	5	0.14	5	0.16	6	0.09	7	0.13	7	0.09	10	0.08	11
strat. nom	0.18	6	0.13	9	0.08	7	0.08	9	0.07	5	0.09	9	0.09	39	0.11	0
strat. gro	0.42	0	0.54	0	0.49	0	0.55	0	0.22	0	0.39	0	0.18	1	0.25	1
strat. run	0.12	14	0.17	12	0.05	11	0.07	13	0.05	17	0.11	13	0.18	0	0.18	0
strat. res	0.17	6	0.16	6	0.17	6	0.17	7	0.08	5	0.12	8	0.10	39	0.09	37
$\delta^{13}CH_4$																
global nom	0.16	1	0.16	50	0.14	2	0.09	50	0.24	46	0.25	39	0.13	3	0.05	50
global gro	0.20	39	0.14	42	0.16	39	0.13	43	0.28	49	0.20	15	0.12	41	0.10	0
global det	0.18	11	0.15	13	0.15	11	0.12	13	0.32	12	0.24	15	0.11	15	0.08	17
global det-gro	0.14	40	0.13	58	0.13	58	0.12	59	0.28	49	0.14	59	0.16	15	0.10	16
BHD nom	0.10	56	0.09	60	0.04	0	0.05	0	0.10	55	0.14	60	0.05	42	0.04	39
BHD gro	0.07	61	0.10	60	0.08	0	0.09	1	0.08	2	0.14	1	0.14	45	0.17	47
BHD run	0.10	0	0.13	0	0.11	0	0.13	0	0.09	62	0.18	57	0.04	38	0.06	41
BHD res	0.05	6	0.05	9	0.06	7	0.05	9	0.06	6	0.04	10	0.07	35	0.05	9
BHD det-nom	0.07	8	0.02	7	0.03	7	0.02	8	0.06	6	0.02	9	0.05	42	0.04	34
BHD det-gro	0.10	0	0.13	0	0.13	0	0.15	1	0.07	2	0.13	0	0.12	45	0.14	47
BHD det-run	0.10	9	0.13	10	0.11	10	0.14	12	0.06	9	0.10	12	0.18	33	0.23	34

Biogeosciences Discuss., https://doi.org/10.5194/bg-2018-304
Manuscript under review for journal Biogeosciences
Discussion started: 24 July 2018

ASC nom	0.09	54	0.08	58	0.04	54	0.04	37	0.09	55	0.16	33	0.04	52	0.03	32
ASC gro	0.10	14	0.14	14	0.08	13	0.10	13	0.08	12	0.19	13	0.15	5	0.22	7
ASC run	0.07	51	0.11	54	0.04	50	0.06	53	0.09	51	0.20	27	0.05	22	0.08	23
ASC res	0.03	17	0.04	22	0.03	18	0.02	19	0.05	29	0.07	24	0.04	14	0.03	18
ASC det-nom	0.06	18	0.04	22	0.03	18	0.01	18	0.06	29	0.05	32	0.05	15	0.02	17
ASC det-gro	0.07	14	0.08	14	0.04	13	0.05	59	0.05	13	0.09	14	0.07	8	0.10	7
ASC det-run	0.07	22	0.09	23	0.04	59	0.05	59	0.07	25	0.16	24	0.06	56	0.08	57
SMO nom	0.07	56	0.08	54	0.03	45	0.04	45	0.09	42	0.14	45	0.05	41	0.05	39
SMO gro	0.04	66	0.04	67	0.04	66	0.03	25	0.03	0	0.06	0	0.10	43	0.11	43
SMO run	0.07	50	0.10	49	0.03	38	0.05	0	0.09	51	0.18	49	0.03	38	0.04	35
SMO res	0.10	0	0.07	2	0.10	1	0.07	3	0.10	1	0.06	5	0.06	14	0.06	16
SMO det-nom	0.07	0	0.06	2	0.08	1	0.05	3	0.07	1	0.05	5	0.06	14	0.05	16
SMO det-gro	0.05	22	0.05	24	0.05	66	0.06	25	0.02	26	0.03	26	0.06	42	0.07	42
SMO det-run	0.06	1	0.06	2	0.07	2	0.08	3	0.05	15	0.07	16	0.14	16	0.19	20